Spray Coating Experiments: Setups and Methodologies
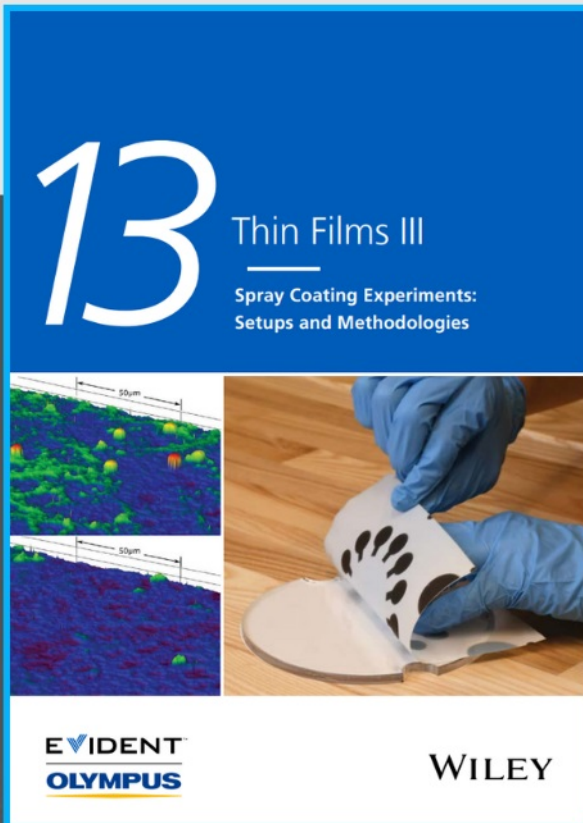

13

Thin Films III

Spray Coating Experiments: Setups and Methodologies

EVIDENT OLYMPUS

WILEY

The latest eBook from Advanced Optical Metrology. Download for free.

Spray Coating Experiments: Setups and Methodologies, is the third in our Thin Films eBook series. This publication provides an introduction to spray coating, three article digests from Wiley Online Library and the latest news about Evident's Image of the Year Award 2022.

Wiley in collaboration with Evident, are committed to bridging the gap between fundamental research and industrial applications in the field of optical metrology. We strive to do this by collecting and organizing existing information, making it more accessible and useful for researchers and practitioners alike.

EVIDENT OLYMPUS

WILEY

RESEARCH ARTICLE

A Neuron-Readable Artificial Photoreceptor Composed of Photodeformable Liquid Crystal Polymers and Piezoelectric Materials

Bo Peng, Xueli Chen, Guodong Yu, Fan Xu, Ruyi Yang, Zhenghang Yu, Jia Wei, Guodong Zhu, Lang Qin, Jiayi Zhang, Qundong Shen, and Yanlei Yu*

Artificial photoreceptors are extensively developed to help the patients with serious eye diseases by converting light into electric signals. However, the existing systems still suffer from poor output signals, restricting signal transduction to cells. Here, a neuron-readable artificial photoreceptor with significant voltage output is constructed by using photodeformable liquid crystal polymers (LCPs) and polyvinylidene fluoride trifluoroethylene (P(VDF-TrFE)). The significant voltage output originates from light-stress-electricity conversion, where the photo-induced stress is attributed to the free volume expansion of the photodeformable LCPs and subsequently converts them into strong electric signals by the P(VDF-TrFE) layer. The photo-induced open-circuit voltage reaches up to 0.79 ± 0.02 V, which is, to the knowledge, 19 times higher than the maximum voltage (0.04 V) that has been reported to date. Hence, such artificial photoreceptor successfully transduces photo-induced electric signals to cells and tissues, communicates with the neurons, and triggers spiking activities in blind retinas. Besides, visual image recognition is demonstrated in a pixelated matrix by analyzing electric signals of each unit. This artificial photoreceptor opens new opportunities for the combination of the photodeformability and piezoelectricity, providing an avenue to develop neuron-readable artificial retinas and implantable sensors.

1. Introduction

The photoreceptor generating electric signals when stimulated by light is an important organ for animals to obtain external information.[1] Developing artificial photoreceptors will provide an effective strategy to deal with serious eye diseases such as retinitis pigmentosa and macular degeneration.[2] The

researchers focus on the development of intelligent materials and novel mechanism in the new-generation photoreceptors to simplify the camera visual systems like Argus II.[3] Photovoltaic materials such as cadmium sulfide nanorods,[4] single-crystalline silicon photodiodes,[5] output photoelectric signals by the generation and migration of the photocarrier, but the reactive oxygen generated in photoelectrical conversion process is concerned with cytotoxicity and limits the organism application. Pyroelectric materials such as ZnO,[6] poly(vinylidene fluoride-co-hexafluropropylene)[7] are used for electric power output under NIR by the spontaneous polarization change with temperature; however, the photothermal effect of NIR limits the miniaturization of devices.

The conversion of light-stress-electric signals can be realized by the combination of photodeformable materials and piezoelectric materials, which provides an opportunity for the construction of novel artificial photoreceptors without above-mentioned disadvantages. Azobenzene moieties are usually used as a trigger to generate photo-induced stress in the polymers by *trans–cis* isomerization upon exposure to light irradiation. Combined with azobenzene polymers, the piezoelectric polymers convert the stress into electric signals due to the density change of dipoles. Shen et al. blended azobenzene polymers into piezoelectric polymers to obtain a hybrid film, whose

B. Peng, X. Chen, G. Yu, J. Wei, L. Qin, Y. Yu
Department of Materials Science and State Key Laboratory of
Molecular Engineering of Polymers
Fudan University
220 Handan Road, Shanghai 200433, China
E-mail: ylyu@fudan.edu.cn

F. Xu, G. Zhu
Department of Materials Science
Fudan University
220 Handan Road, Shanghai 200433, China

R. Yang, J. Zhang
State Key Laboratory of Medical Neurobiology
MOE Frontiers Center for Brain Science
Institutes of Brain Science
Fudan University
Shanghai 200032, China

Z. Yu, Q. Shen
Department of Polymer Science and Engineering
School of Chemistry and Chemical Engineering
Nanjing University
Nanjing 210023, China

2214172 (1 of 9)

relative capacitance changed by only 1.5% under light irradiation by conversion of light-stress-electric signals.[8] White et al. developed a photopiezoelectric composite to output a small voltage of 6 mV caused by bending under visible light stimulation, where the azobenzene-containing polyimides and polyvinylidene fluoride (PVDF) films were stuck in cantilever geometry by glue.[9] Similarly, Wu et al. developed a composite film of azobenzene-containing agarose and PVDF, which bent under sunlight irradiation and generated voltage with a small value of 40 mV.[10] The low voltage output by conversion of light-stress-electric signals is attributed to the small photo-induced stress and may hinder further application in artificial photoreceptors.

Azobenzene-containing liquid crystal polymers (LCPs) provide a feasible solution to improve the photo-induced stress and output large electric signals because the microscopic geometry variation of azobenzene moieties can be amplified into a macroscopic large deformation of the entire LCP materials.[11] Much effort has been made to develop photoresponsive soft actuators with the azobenzene-containing LCPs by utilizing their quick and various deformation,[12] including contraction/expansion,[13] bending,[14] twisting,[15] etc. Due to the cooperative effect of the LC mesogens, as long as 1 mol% of azobenzene moieties reach the photostationary state upon illumination, the generated alignment change can lead to the deformation of the whole LCP systems. Besides, Broer et al. enhanced mechanical deformation by introducing the dynamics of the *trans-cis-trans* oscillation of the azobenzene moieties in relation to free volume expansion.[16] The oscillation of the *trans-cis-trans* isomerization triggered by blue light created volumetric space of the azobenzene moieties and resulted in volume increase of the whole system.[17] Therefore, photodeformable LCPs are an excellent candidate for the construction of the photoreceptor featuring a large photo-induced stress.[18]

Herein, we report an artificial photoreceptor composed of photodeformable LCPs and piezoelectric materials, which converts visible light into great electric signals (**Figure 1**a). The photodeformable layer is on the top of the artificial photoreceptor which maximizes the absorbance of light irradiation and the piezoelectric layer is sandwiched between two conductive electrodes. Based on the conversion of light-stress-electric signals, the open-circuit voltage has greatly increased to 0.79 ± 0.02 V due to the large photo-induced stress without any thermal effect, which is about ten times as much as the membrane potential difference of nerves.[19] Compared with previously-reported work by conversion of light-stress-electric signals, the open-circuit voltage increases 19 times.[10] It is rather remarkable that the light response of cells and spiking activities have been achieved with our artificial photoreceptor, indicating the direct transduction from the photoreceptor to neurons and tissues. Moreover, the artificial photoreceptors are able to be integrated into the pixelated matrix easily and realize visual image recognition, showing great potential in the fields of neuron-readable artificial retina, implantable sensors, and detectors.

2. Results and Discussion

The artificial photoreceptor used in this work contains four layers on the glass substrate, including the photodeformable

layer, the piezoelectric layer, and two conductive electrodes. The linear liquid crystal polymer (LLCP) with flexible backbones and azobenzene moieties is chosen as the photodeformable layer (Figure 1b; Figures S1 and S2, Supporting Information),[21] which is able to self-assemble into a highly ordered structure due to the molecular cooperation effect of liquid crystals and the free volume of the long spacers (Figure S3, Supporting Information). The free volume expansion via oscillation of the *trans-cis-trans* isomerization in LLCP is beneficial to large and reversible deformation, leading to large photo-induced stress in the conversion from light to stress.[15,21] LLCP also has good processing properties to be prepared as films through the solution method ascribing to its linear structure without any chemical crosslinking, which is also easily combined with other layers when heated above the clearing point. Polyvinylidene fluoride trifluoroethylene (P(VDF-TrFE)) with the high content of β crystal form is selected as the piezoelectric layer because of the outstanding conversion efficiency from stress to electric signals. P(VDF-TrFE) is easy to form homogeneous films by spin-coating, which has been widely used in electromechanical sensors and actuators.[22] During the fabrication of the artificial photoreceptor, the conductive electrode (Al) was evaporated on both sides of the P(VDF-TrFE) layer to enhance the charge accumulation (Figure 1c). The SEM photograph shows no obvious crack at the junction area among different layers, demonstrating the tight and seamless combination of the multi-layer structure (Figure 1d). Under the illumination of 470 nm light, the photo-induced stress generated in the LLCP layer is transferred to the P(VDF-TrFE) layer, where the density change of dipoles leads to the charge redistribution between the two electrodes and the output of the electric signals (Figure 1e).

To investigate the deformation of the LLCP film, its two ends were attached on two separate glass substrates by heating at 95 °C. The film generated cambered bending owing to the surface expansion triggered by 470 nm light because of the free volume expansion via oscillation of the *trans-cis-trans* isomerization (**Figure 2**a). As the UV–vis absorption spectrum of LLCP in the dichloromethane solution shows (Figure S4, Supporting Information), the absorption bands of the n-π* transition of the *trans* form and the n-π* transition of the *cis* form are overlapped ≈470 nm.[23] Therefore, the azobenzene moieties undergo both *trans–cis* and *cis–trans* isomerization under the illumination of 470 nm. The repeated *trans-cis-trans* isomerization cycles further lead to free volume expansion and thus generate photo-induced stress.[24] To verify the free volume expansion of the LLCP film triggered by 470 nm light, we measured density of a free-standing film in the illuminated and unilluminated state (Figure S5 and Movie S1, Supporting Information). The LLCP film sunk at the bottom of cuvette when immersed in the salt brine with a density of 1.042 g cm^{-3}, which was lower than that of the film. The film started floating upon the illumination of 470 nm light and sunk as soon as the light was switched off. The "sink-float-sink" process is repeatable as three cycles, indicating the density decrease of the LLCP film upon illumination, which is ascribed to the free volume expansion via oscillation of the *trans-cis-trans* isomerization.

To confirm that the deformation of the LLCP film was not generated by photothermal effect, the IR thermography was carried out to measure the temperature change during the
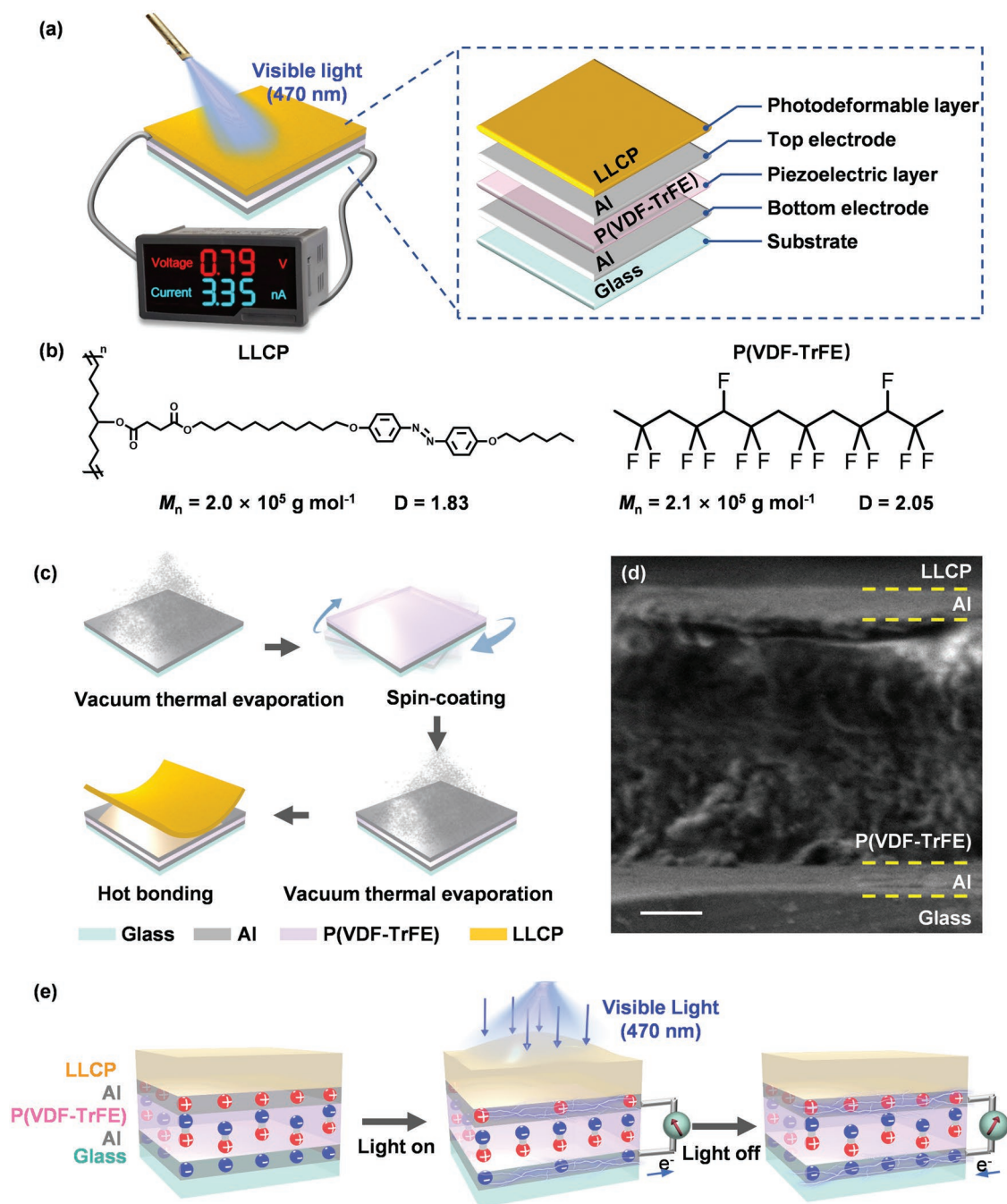
Figure 1. a) Schematic illustration to show the multi-layer structure of the artificial photoreceptor. Under the illumination of visible light, the artificial photoreceptor outputs the stable open-circuit voltage of 0.79 V and short-circuit current of 3.35 nA. b) Molecular structures of liner liquid crystal polymer (LLCP) and polyvinylidene fluoride trifluoroethylene (P(VDF-TrFE)). c) Schematic illustration to show the fabrication of the artificial photoreceptor. d) SEM photograph of the cross section of the artificial photoreceptor. The scale bar is 500 nm. e) Schematic illustration to show the conversion of light-stress-electric signals. The LLCP layer expands under the illumination and generates the photo-induced stress. The density change of dipoles leads to the charge redistribution between the two electrodes and the output of electric signals.

illumination. The temperature at the light spot increases by only ≈2.2 °C, which is too low to induce the phase transition and the deformation of the LLCP film (Figure S6, Supporting Information). The displacement of the LLCP film (defined as the distance from the top of the camber to its original position) reaches as large as 105 μm with the light intensity of

80 mW cm^{-2}, and the bent film reverses to its original shape when the light is removed (Movie S2, Supporting Information). In this case, the deformation and reversion process has no obvious fatigue even after 55 repetitions, showing good repeatability of the photodeformable film (Figure S7, Supporting Information).
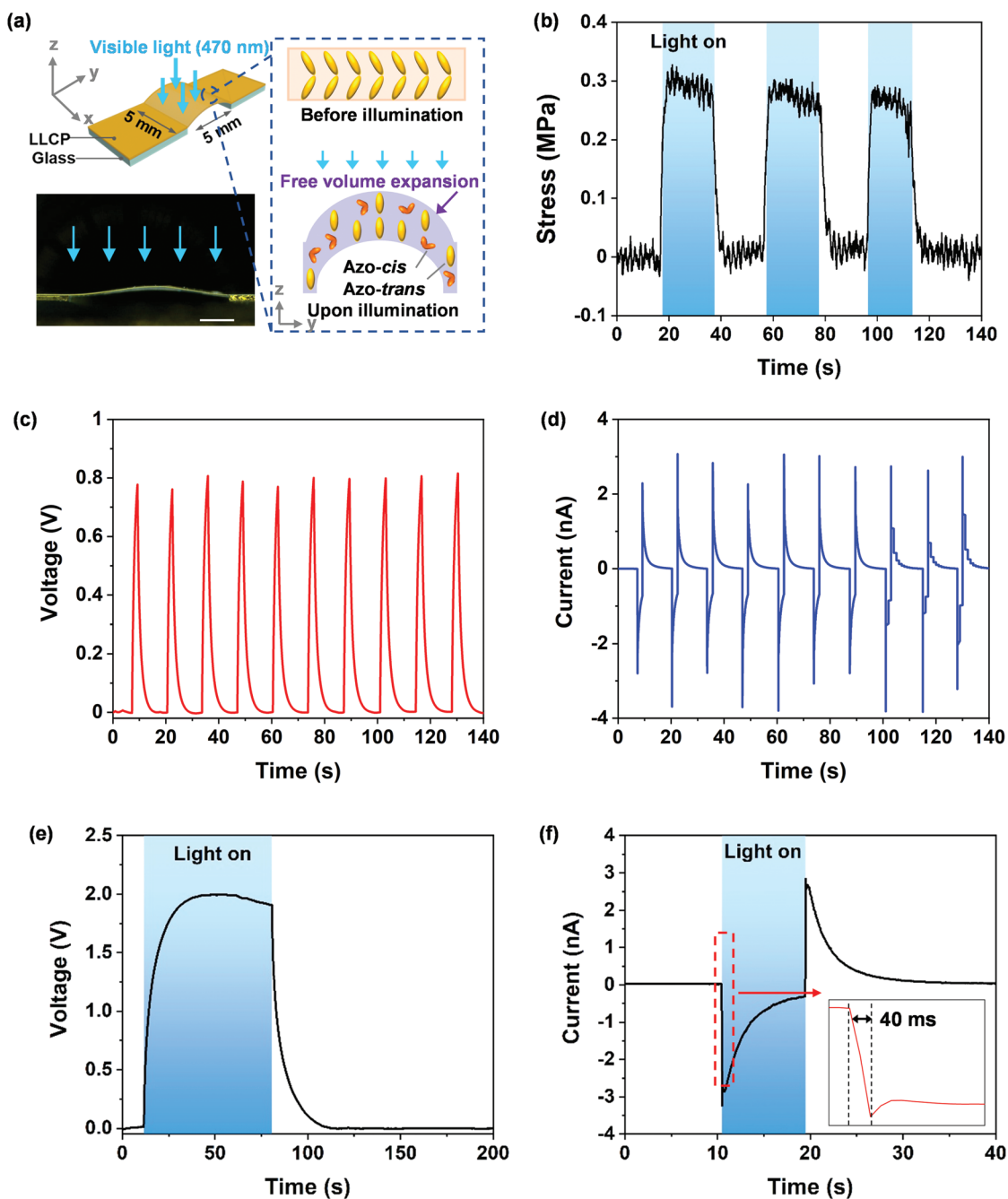
Figure 2. a) Lateral view photograph of the LLCP film deformation and the mechanism under the illumination of 470 nm light. Two ends of the LLCP film are attached on the glass substrates by heating. The thickness of the film is 20 µm. The scale bar is 1 mm. b) Plot showing the photo-induced stress of the LLCP film under 470 nm light (80 mW cm^{-2}). The size of the LLCP film is 10 mm × 5 mm × 20 µm. c) Plot showing the open-circuit voltage of the artificial photoreceptor during ten cycles. d) Plot showing the short-circuit current of the artificial photoreceptor during ten cycles. The duration of illumination and interval are 2 and 10 s, respectively. e) The open-circuit voltage output curve under the illumination for 70 s. The intensity of 470 nm light is 80 mW cm^{-2}. f) The short-circuit current output curve upon illumination for 10 s. The inset shows the response time within 40 ms. The blue column indicates the duration of illumination.

The photo-induced stress is evaluated by tensile machine, where both ends of the LLCP film are clamped and 2 MPa is added as an initial load. The change of the load resulting from the film expansion is measured under the illumination and the value of the photo-induced stress reaches 0.3 MPa at 80 mW cm^{-2} (Figure 2b), which is close to the stress of vertebrate muscle fibers (0.35 MPa).[25] The photo-induced stress of the LLCP film increases with increasing intensity of 470 nm light and reaches a plateau at 80 mW cm^{-2} (Figure S8, Supporting Information), which is in agreement with the change tendency of the deformation of the LLCP film (Figure S9, Supporting Information).

The open-circuit voltage and short-circuit current of the artificial photoreceptor are detected during ten cycles (Figure 2c,d), clarifying that the photo-induced stress is transferred from the LLCP layer to the P(VDF-TrFE) layer. At the moment of turning on and off the 470 nm light, the short-circuit current changes the direction to generate positive and negative peaks (Figure 2d), which results from the generation and disappearance of the photo-induced stress. With continuous illumination of the 470 nm light, the value of the open-circuit voltage remains unchanged, indicating the stable potential difference between two electrodes (Figure 2e). It is noted that compared to the response of human eyes ranging from 50 to 150 ms,[26] our artificial photoreceptor responds in 40 ms (Figure 2f), which is attributed to the fast photoisomerization of azobenzene moieties in the order of milliseconds.[27] When the temperature of the artificial photoreceptor was increased by 2.2 °C, the electric signals remained unchanged, indicating the increase of temperature did not generate the pyroelectric-induced signals. Similarly, no obvious signals of the artificial photoreceptor without the LLCP layer being observed under the illumination of 470 nm light, which means the stress generated by the free volume expansion in the LLCP layer is indispensable for the artificial photoreceptor (Figures S10 and S11, Supporting Information).

The electric signals of the artificial photoreceptor are closely related to the photo-induced stress, which can be regulated with the light intensity. When increasing the light intensity from 19 to 80 mW cm^{-2} with a 2 s duration and 10 s intervals,

both the peak value of short-circuit current and open-circuit voltage increase (**Figure 3**a,b). It is worth noting that the peak value of short-circuit current and open-circuit voltage are both proportional to the light intensity (Figures S12 and S13, Supporting Information). The open-circuit voltage reaches up to 0.79 ± 0.02 V under 80 mW cm^{-2} illumination (Figure 3b), which is 19 times higher than the maximum voltage (0.04 V) that has been reported without LCPs by the conversion of light-stress-electric signals.[10] The significant electric signals are ascribed to both the free volume expansion via oscillation of the trans-cis-trans isomerization, and the seamless joint which reduces losses during the photo-induced stress transfer. By utilizing LCPs, Chen et. al. demonstrated a UV monitor with a relative current change of 40% based on ionic liquids (ILs) and LCPs. The LCP fibers deformed under UV light and transferred the UV light-triggered stress to ILs and then the ions migrated to output current in 5 s.[28] However, the trigger conditions of UV light and slow response limit the application in artificial photoreceptors. Combing the photodeformability of LLCP and piezoelectricity of P(VDF-TrFE), the response time of our new artificial photoreceptor reaches up to 40 ms under visible light, faster than that of human eyes.

The influence of the illumination time from 2 to 10 s on the short-circuit current and open-circuit voltage was also investigated. When turning on the 470 nm light, the short-circuit current immediately reaches the negative peak, which turns to the positive peak after removing the light. The peak value of short-circuit current is almost the same as we prolong the
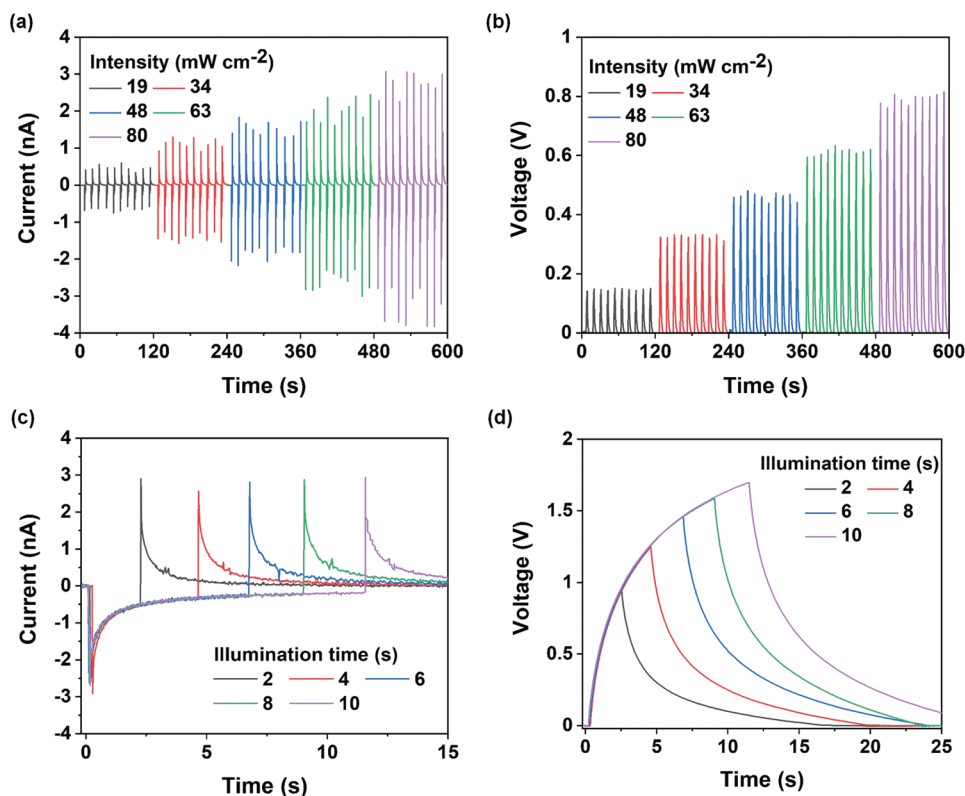
Figure 3. a) The short-circuit current and b) the open-circuit voltage of the artificial photoreceptor under 470 nm light with different light intensities. The duration of illumination and interval are 2 and 10 s, respectively. c) The short-circuit current and d) the open-circuit voltage of the artificial photoreceptor under 470 nm light for different illumination times. The intensity of the light is 80 mW cm^{-2}.
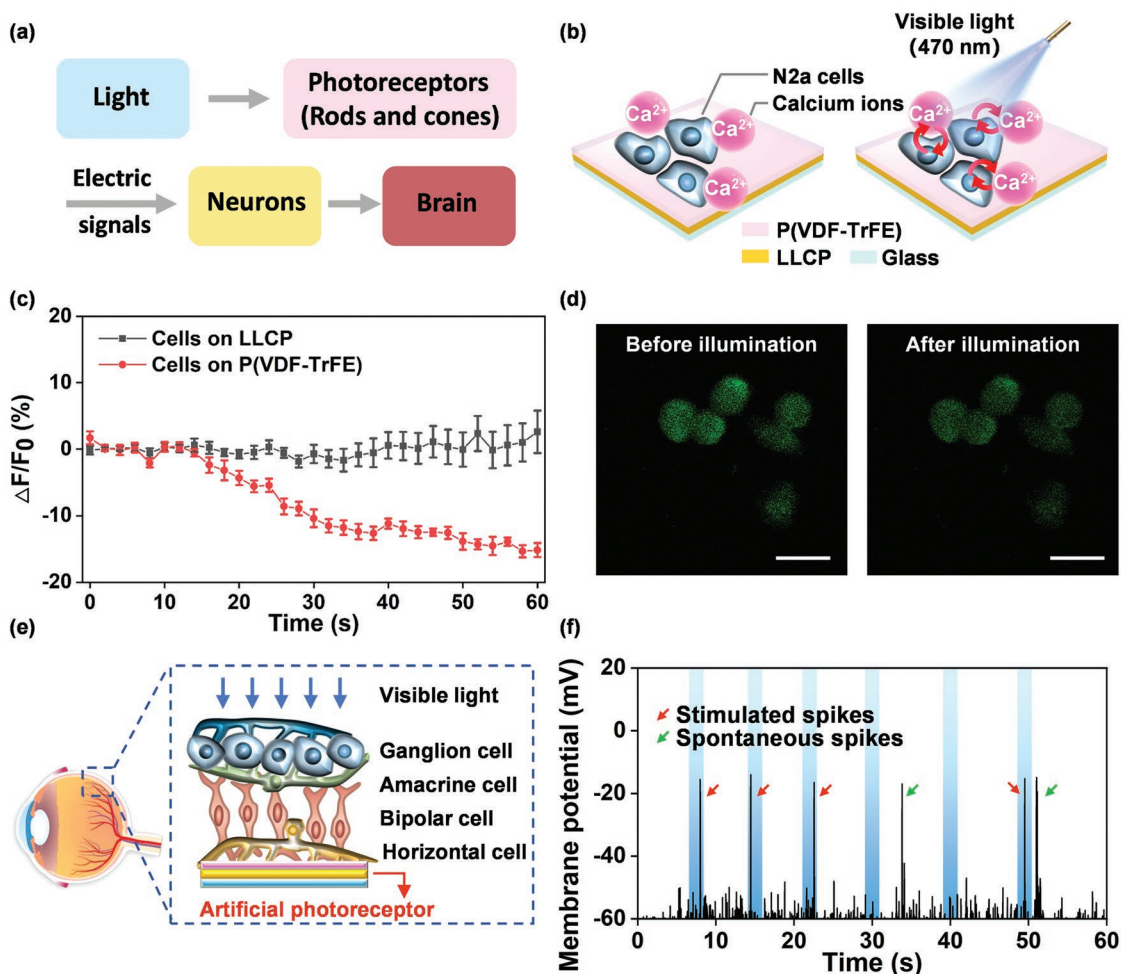
Figure 4. a) Signal transduction from the photoreceptor cells to the neuron cells in human visual system. b) Schematic illustration of the signal transduction from the photoreceptor to the GCamp6-GFP N2a cells. The cells are incubated on the surface of the P(VDF-TrFE) layer. c) The change of relative fluorescence intensity for the cells incubated on the different layers. d) Calcium imaging of the GCamp6-GFP N2a cells before and after 470 nm light illumination (80 mW cm^{-2}) for 60 s. The scale bar is 50 μm. e) Schematic illustration of the blind retina that lacks photoreceptors. The necrotic photoreceptor layer (rod and cone cells) in the blind retina is replaced by the artificial photoreceptor. f) Light responses of retinal ganglion cells (RGCs) in the blind retina with the artificial photoreceptor. The retina is on the top of the artificial photoreceptor. The red and green arrows stand for the stimulated and spontaneous spiking activities, respectively. The blue columns indicate 470 nm light illumination (80 mW cm^{-2}) for 2 s.

illumination time (Figure 3c) because the photo-induced stress is generated at the moment of turning on the light and remains unchanged until removing the illumination. The value of the open-circuit voltage increases with the illumination time until reaching the new equilibrium of charge (Figure 3d), which requires ≈40 s to obtain unchanged voltage (Figure 2e).

Similar as the signal transduction in human visual system (**Figure 4**a), the transduction process was demonstrated from artificial photoreceptors to neuron cells. Calcium ions that generate versatile intracellular signals control key functions in all types of neurons. The influx of Ca ions between extracellular environment and intracellular stores reflects neuronal activities,[29] which is able to be detected via the relative fluorescence intensity change of the cells. The calcium imaging of the cells under 470 nm illumination was carried out by a fluorescent probe and confocal microscopy. GCamp6-GFP N2a cells as a neuron cell model are incubated on the surface of P(VDF-TrFE) layer, where the photoelectric signals in the artificial

photoreceptor without aluminum electrodes will directly stimulate the cells (Figure 4b). Omitting the electrodes not only allows the light to go through the transparent P(VDF-TrFE) layer to the LLCP layer but also ensures the direct contact of cells and P(VDF-TrFE) layer to transduce photoelectric signals. The 470 nm light penetrates the cells from the top and arrives at the P(VDF-TrFE) layer, which is similar to the real visual process in human eyes, i.e., visible light propagates through the cells in retinas and arrives at photoreceptor cells. On the other hand, we set a control group where the cells are incubated on the insulative LLCP layer surface. Figure 4c shows the relative fluorescence intensity change of the cells, where the light intensity of 80 mW cm^{-2} is chosen to efficiently stimulate the neurons. During the illumination for 60 s, the calcium-ion concentrations of cells on the P(VDF-TrFE) layer decrease, which indicates that the balance of cytosolic calcium concentration is broken between the calcium influx and efflux, resulting from the communication between the artificial photoreceptor

and cells. Although the open-circuit voltage (0.79 V) is much higher than the membrane potential difference of nerves,[19] the calcium flux of the cells on LLCP layer changes little because the insulative layer blocks the photoelectric signals from the P(VDF-TrFE) layer to stimulate the cells. Figure 4d shows the fluorescence images of the cells on the P(VDF-TrFE) layer after illumination for 60 s, showing ≈15% decrease in relative fluorescence intensity.

To further clarify the photoelectric signal transduction in retinal tissues, the artificial photoreceptor is interfaced with retinal degenerated 1 (rd1) /cone diphtheria toxin subunit-A (cDTA) blind mouse retinas (Figure 4e). The necrotic photoreceptor layer (rod and cone cells) in the blind retina is replaced by the artificial photoreceptor and light responses of retinal ganglion cells (RGCs) are recorded by whole-cell patch clamp pipettes (Figure S14, Supporting Information). The RGCs in enucleated retinas still have spontaneous spiking activities, indicating the good state of cells in vitro. To avoid the confusion of spontaneous and stimulated spiking activities, a short duration of 2 s is chosen instead of continuous illumination. Most of the illumination successfully stimulates the RGCs and elicits the spikes as indicated with red arrows in Figure 4f, whereas the green arrows stand for the spontaneous spiking activities beyond the illumination. It is clear that the RGCs responses are closely correlated with the light stimulation, indicating the transduction in blind retinal tissues. The above results exhibit the messenger exchange process among neuron cells, retinal tissues, and the environment under the stimuli of the artificial photoreceptor, which is similar to the signal transduction in human retinas.

Inspired of the human visual system which has ≈100–120 million photoreceptors vertically assembled in the retina for optical sensing with a spatial resolution ≈5000 PPI,[30] the artificial photoreceptors are integrated into a pixelated matrix with 25 units (5 × 5 mm for each unit) as shown in **Figure 5**a, which is necessary for visual image recognition rather than detecting the light on- or off- state by single artificial photoreceptor. The fabrication of the pixelated matrix is the same as the single artificial photoreceptor by using patterned mask for evaporating electrodes, where the nonoverlapping electrode lines avoid the interfere among different pixel units with careful design (Figure 5b; Figure S15, Supporting Information). The short-circuit current of each single pixel is collected, where the light goes through the carved area in the patterned photomask to carry information of letters and numbers (Figure 5c). The values of short-circuit current are measured by histogram in Figure 5d,e to display the image, and the clear "F" and "9" patterns are obtained. The values in the illuminated pixel units (≈2.80 nA) are 21 times higher than those in blocked units (≈0.13 nA), which lays the foundation for the accuracy of the visual image recognition. In addition, the electric signals have good linear correlation to the optical signals (Figures S12 and S13, Supporting Information), which may be expected to realize the visual image recognition with different light intensities, promoting the construction and development of artificial vision systems.

3. Conclusion

In summary, we have combined LLCP and P(VDF-TrFE) to fabricate an artificial photoreceptor with great electric signals, where

the ordered azobenzene mesogens in the LLCP layer undergo *trans-cis-trans* isomerization repeatable cycles under the illumination of 470 nm light to generate significant free volume expansion and photo-induced stress. Then the photo-induced stress is transferred to the P(VDF-TrFE) layer, where the density change of dipoles leads to the charge redistribution and electric signals. The photo-induced open-circuit voltage reaches up to 0.79 ± 0.02 V, which originates from light-stress-electricity conversion. More importantly, the artificial photoreceptor directly transduced the electric signals to the neuron cells and triggered spiking activities in photoreceptor-degenerated retinal tissue in vitro, helping rsestore the blind retinas. By integrating 25 single artificial photoreceptors, the pixelated matrix was obtained and successfully recognized the visual image due to the large value difference between the illuminated and blocked pixel units. We believe that our work will facilitate the development of future investigations on implantable devices of the LCPs, and open up new vistas for neuron-readable artificial retinas as well as intelligent detectors.

4. Experimental Section

Materials: All chemicals were used as received without further purification. polyvinylidene fluoride trifluoroethylene (P(VDF-TrFE)) (70/30 mol⁻¹) was purchased from Kunshan Hisense Electronic Co. (Shanghai). Liner liquid crystal polymer (LLCP) was synthesized from previously reported method.[20] GCamp6-GFP mouse neuroblastoma N2a cell line (GCamp6-GFP N2a cells), Dulbecco's modified Eagle medium (DMEM), and Fluo-4 AM were purchased from KeyGen BioTECH (Jiangsu, China).

Fabrication of the Artificial Photoreceptor and Pixelated Matrix: The artificial photoreceptor was fabricated in a four-step method: 1) The aluminum (Al) was vacuum thermally evaporated on a clean glass substrate as the bottom electrode. 2) P(VDF-TrFE) (10% m/v) was dissolved in cyclopentanone and then spin-coated on the bottom electrode to form a piezoelectric film, subsequently annealed at 135 °C for 3 h. 3) The top electrode of aluminum was vacuum thermally evaporated. 4) LLCP in dichloroethane (5% w/w) was additionally drop-coated on the glass substrate and annealed at 55 °C for 3 h before peeling the film. The artificial photoreceptor was fabricated by attaching the LLCP film to the surface of the top electrode at 95 °C on a hot stage. The pixelated matrix was obtained similarly with a designed patterned mask by the four-step method.

Characterization of LLCP: Textures of the LLCP were observed on a polarized optical microscope (POM, Leica DM2500P). 2D-WAXD experiments on the LLCP films were conducted on Xeuss 2.0 system (Xenocs). The photo-induced stress of LLCP was performed on an Instron Testing Machine (Model 5943) at room temperature. The film deformation of LLCP was measured in the super-resolution digital microscope with an analysis software (Keyence, VHX-1000C). UV–vis absorption spectra were obtained using a Lambda 650 UV/Vis spectrometer (Waltham, MA, USA).

Electric Signal Measurement: A 470 nm visible light lamp (CCS, PJ-1505-2CA, HLV-24BL-3 W) was used as blue light source. The short-circuit current and open-circuit voltage of the device were measured by a source meter (Keysight B2902A).

Cell Culture: GCamp6-GFP N2a cells were seeded in dishes on the LLCP or P(VDF-TrFE) layer. Then the cells were cultured in DMEM medium supplemented with 10% fetal bovine serum and 1% penicillin antibiotic. These cells were incubated under a fully humidified atmosphere at 37 °C with 5% CO₂.

Calcium Imaging: Fluo-4 AM (1 × 10⁻⁶ M) was dissolved in DMEM without serum and GCamp6-GFP N2a cells were incubated in that for 30 min at 37 °C. Then the samples were washed and supplied with artificial cerebrospinal fluid (aCSF). The aCSF contained NaCl 140 mM,
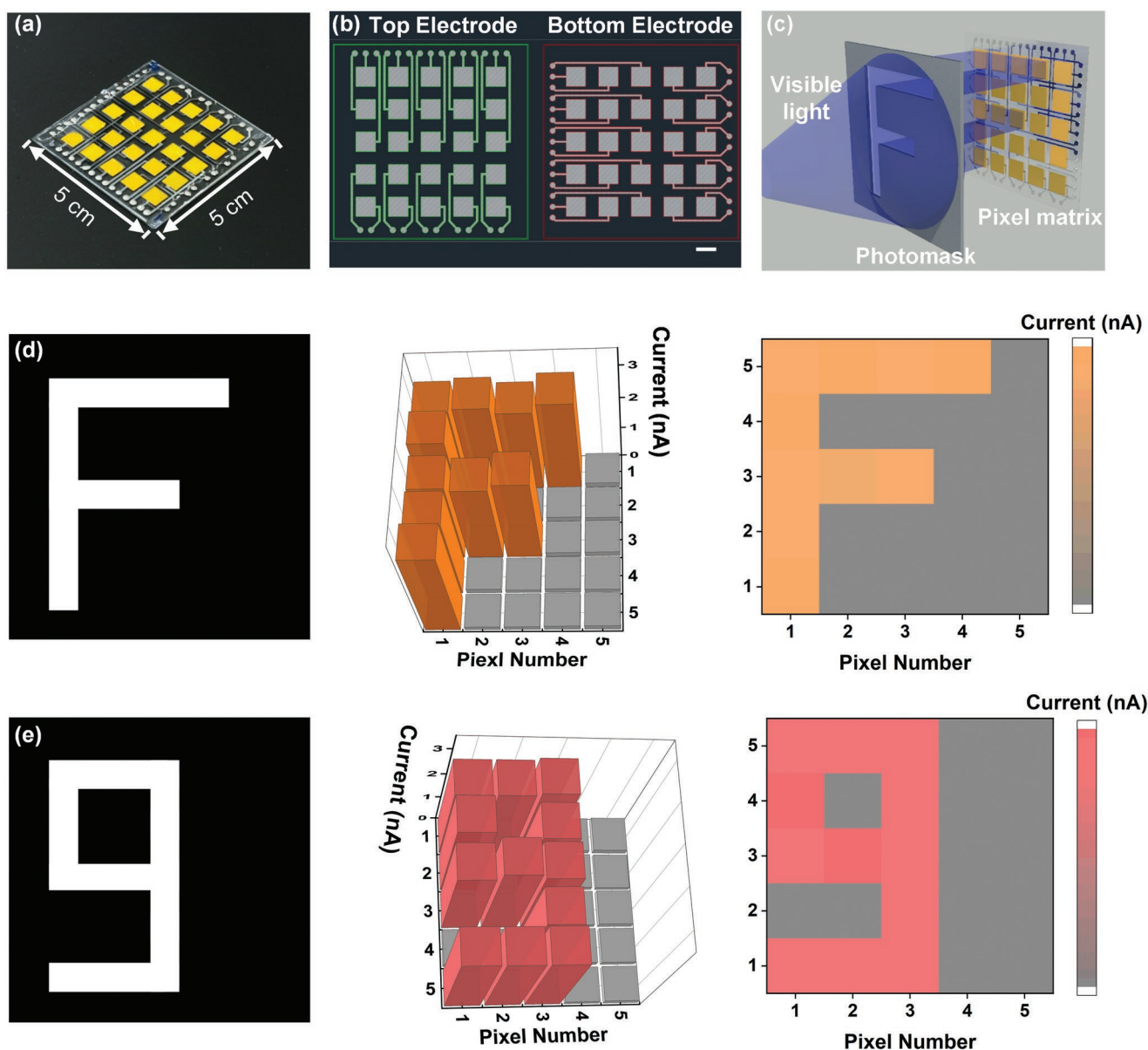
Figure 5. a) The photograph of the pixelated matrix with 25 units. Each unit is an independent artificial photoreceptor. b)The electrode design of the 5 × 5 pixelated matrix. c) Schematic illustration of the visual image recognition. The pixelated matrix is illuminated by the light through the patterned photomask. Plot showing the short-circuit current in pixelated matrix with the pattern d) "F" and e) "9".

KCl 5 mM, CaCl$_2$ 2 mM, MgCl$_2$ 2 mM, HEPES 10 mM, and d-glucose 10 M, pH = 7.4. 470 nm light (80 mW cm^{-2}) was illuminated on the samples for 60 s. The images were collected in the illumination process with an inverted fluorescence microscope (Olympus IX81). The excitation filter is 460–480 HQ and the emission filter is 495–540 HQ. The integrated optical density of each cell was obtained by Image-Pro Plus software.

Retinal Tissue Preparation and Patch-Clamp Recording: All procedures were conducted in accordance with the guidelines of the Institutional Animal Care and Use Committee at Shanghai Public Health Clinical Center. All protocols for mouse experiments were approved by the Animal Ethics Committee of School of Basic Medical Science at Fudan University (20200306-139). Mice were anesthetized with 10% chloral hydrate (0.3 mL per 100 g weight). One eye was enucleated and rapidly placed in Ringer's solution which contained NaCl 124 mM, KCl 2.5 mM, CaCl$_2$ 2 mM, MgCl$_2$ 2 mM, NaH$_2$PO$_4$ 1.25 mM, NaHCO$_3$ 26 mM, and glucose 22 mM, pH = 7.35, oxygenated with 95% O$_2$ and 5% CO$_2$. Then the retina was dissected and placed on a filter paper (MerckMillipore, Germany) in the recording chamber. Action potentials were recorded by MultiClamp 700B patch-clamp amplifier (Molecular Devices, USA) and digitized by Digidata 1440 (Molecular Devices, USA) under DIC microscope (Zeiss, Germany) at 25 °C. A glass pipette (5–10 MΩ) was pulled by P-97 micropipette puller (Sutter Instruments, USA) filled with potassium gluconate 105 mM, KCl 5 mM, CaCl$_2$ 0.5 mM, MgCl$_2$ 2 mM, EGTA 5 mM, HEPES 10 mM, Mg-ATP 4 mM, GTP-Na 0.5 mM, sodium phosphocreatine 7 mM, Lucifer Yellow 0.05%, pH = 7.4.

Supporting Information

Supporting Information is available from the Wiley Online Library or from the author.

Acknowledgements

Conflict of Interest

The authors declare no conflict of interest.

Data Availability Statement

The data that support the findings of this study are available in the supplementary material of this article.

[1] a) J. J. Zheng, S. Lee, Z. J. Zhou, *Nat. Neurosci.* **2006**, *9*, 363; b) X. Guo, S.-B. Wang, H. Xu, A. Ribic, E. J. Mohns, Y. Zhou, X. Zhu, T. Biederer, M. C. Crair, B. Chen, *Nat. Commun.* **2015**, *6*, 8005.

[2] a) D. L. Cheng, P. B. Greenberg, D. A. Borton, *Curr. Eye Res.* **2017**, *42*, 334; b) M. S. Humayun, E. de JuanJr., G. Dagnelie, *Ophthalmology* **2016**, *123*, S89.

[3] a) L. da Cruz, B. F. Coley, J. Dorn, F. Merlini, E. Filley, P. Christopher, F. K. Chen, V. Wuyyuru, J. Sahel, P. Stanga, M. Humayun, R. J. Greenberg, G. Dagnelie, I. I. S. G. Argus, *Brit. J. Ophthalmol.* **2013**, *97*, 632; b) J. Wang, Q. Zhao, Y. Wang, Q. Zeng, T. Wu, X. Du, *Adv. Mater. Technol.* **2019**, *4*, 1900566.

[4] L. Bareket, N. Waiskopf, D. Rand, G. Lubin, M. David-Pur, J. Ben-Dov, S. Roy, C. Eleftheriou, E. Sernagor, O. Cheshnovsky, U. Banin, Y. Hanein, *Nano Lett.* **2014**, *14*, 6685.

[5] H. C. Ko, M. P. Stoykovich, J. Song, V. Malyarchuk, W. M. Choi, C.-J. Yu, J. B. GeddesIII, J. Xiao, S. Wang, Y. Huang, J. A. Rogers, *Nature* **2008**, *454*, 748.

[6] Y. Zhu, B. Wang, C. Deng, Y. Wang, X. Wang, *Nano Energy* **2021**, *83*, 105801.

[7] B. Dai, J. Fang, Y. Yu, M. Sun, H. Huang, C. Lu, J. Kou, Y. Zhao, Z. Xu, *Adv. Mater.* **2020**, *32*, 2203057.

[8] X. Chen, S. Pan, P.-J. Feng, H. Bian, X. Han, J.-H. Liu, X. Guo, D. Chen, H. Ge, Q.-D. Shen, *Adv. Mater.* **2016**, *28*, 10684.

[9] J. J. Wie, D. H. Wang, V. P. Tondiglia, N. V. Tabiryan, R. O. Vergara-Toloza, L.-S. Tan, T. J. White, *Macromol. Rapid Commun.* **2014**, *35*, 2050.

[10] Y. Xiong, L. Zhang, P. Weis, P. Naumov, S. Wu, *J. Mater. Chem. A* **2018**, *6*, 3361.

[11] a) Y. Xia, X. Zhang, S. Yang, *Angew. Chem. Int. Ed.* **2018**, *57*, 5665; b) B. Zuo, M. Wang, B.-P. Lin, H. Yang, *Nat. Commun.* **2019**, *10*, 4539.

[12] a) S. Han, Y. Chen, B. Xu, J. Wei, J. Yu, *Chin. J. Polym. Sci.* **2020**, *38*, 806; b) X. Qing, J. Lv, Y. Yu, *Acta Polym. Sin.* **2017**, *11*, 1679.

[13] X. Pang, L. Qin, B. Xu, Q. Liu, Y. Yu, *Adv. Funct. Mater.* **2020**, *30*, 2002451.

[14] a) C. L. van Oosten, C. W. M. Bastiaansen, D. J. Broer, *Nat. Mater.* **2009**, *8*, 677; b) S. Huang, Y. Shen, H. K. Bisoyi, Y. Tao, Z. Liu, M. Wang, H. Yang, Q. Li, *J. Am. Chem. Soc.* **2021**, *143*, 12543.

[15] S. Iamsaard, S. J. Asshoff, B. Matt, T. Kudernac, J. J. L. M. Cornelissen, S. P. Fletcher, N. Katsonis, *Nat. Chem.* **2014**, *6*, 229.

[16] D. Liu, C. Bastiaansen, J. den Toonder, D. J. Broer, *Angew. Chem. Int. Ed.* **2012**, *51*, 892.

[17] D. Liu, D. J. Broer, *Nat. Commun.* **2015**, *6*, 8334.

[18] a) X. Pang, J. Lv, C. Zhu, L. Qi, Y. Yu, *Adv. Mater.* **2019**, *31*, 1904224; b) Y.-C. Cheng, H.-C. Lu, X. Lee, H. Zeng, A. Priimagi, *Adv. Mater.* **2020**, *32*, 1906233.

[19] S. G. Waxman, G. W. Zamponi, *Nat. Neurosci.* **2014**, *17*, 153.

[20] J. Lv, Y. Liu, J. Wei, E. Chen, L. Qin, Y. Yu, *Nature* **2016**, *537*, 179.

[21] Y. Yu, M. Nakano, T. Ikeda, *Nature* **2003**, *425*, 145.

[22] a) B. Chu, X. Zhou, K. Ren, B. Neese, M. Lin, Q. Wang, F. Bauer, Q. M. Zhang, *Science* **2006**, *313*, 334; b) M. A. Fernandez-Yague, A. Trotier, S. Demir, S. A. Abbah, A. Larranaga, A. Thirumaran, A. Stapleton, S. A. M. Tofail, M. Palma, M. Kilcoyne, A. Pandit, M. J. Biggs, *Adv. Mater.* **2021**, *33*, 2008788.

[23] a) F. Weigert, *Verh. Dtsch. Phys. Ges.* **1919**, *21*, 479; b) A. A. Beharry, G. A. Woolley, *Chem. Soc. Rev.* **2011**, *40*, 4422.

[24] a) Q. Liu, G. Yu, C. Zhu, B. Peng, R. Li, T. Yi, Y. Yu, *Small Methods* **2021**, *5*, 2100969; b) Y. Yu, T. Ikeda, *J. Photochem. Photobiol. C* **2004**, *5*, 247.

[25] a) C. S. Haines, M. D. Lima, N. Li, G. M. Spinks, J. Foroughi, J. D. W. Madden, S. H. Kim, S. Fang, M. J. de Andrade, F. Goktepe, O. Goktepe, S. M. Mirvakili, S. Naficy, X. Lepro, J. Oh, M. E. Kozlov, S. J. Kim, X. Xu, B. J. Swedlove, G. G. Wallace, R. H. Baughman, *Science* **2014**, *343*, 868; b) S. Hara, T. Zama, W. Takashima, K. Kaneto, *Polymer J.* **2004**, *36*, 151.

[26] K. Rayner, T. J. Smith, G. L. Malcolm, J. M. Henderson, *Psychol. Sci.* **2009**, *20*, 6.

[27] a) T. Ikeda, O. Tsutsumi, *Science* **1995**, *268*, 1873; b) T. Ikeda, T. Sasaki, H. Kim, *J. Phys. Chem.* **1991**, *95*, 509.

[28] X. Zheng, Y. Jia, A. Chen, *Nat. Commun.* **2021**, *12*, 4875.

[29] a) A. Marino, S. Arai, Y. Hou, E. Sinibaldi, M. Pellegrino, Y.-T. Chang, B. Mazzolai, V. Mattoli, M. Suzuki, G. Ciofani, *ACS Nano* **2015**, *9*, 7678; b) G. Ciofani, S. Danti, D. D'Alessandro, L. Ricotti, S. Moscato, G. Bertoni, A. Falqui, S. Berrettini, M. Petrini, V. Mattoli, A. Menciassi, *ACS Nano* **2010**, *4*, 6267.

[30] a) J. J. Nassi, E. M. Callaway, *Nat. Rev. Neurosci.* **2009**, *10*, 360; b) J. B. Jonas, U. Schneider, G. O. H. Naumann, *Graefes Arch. Clin. Exp. Ophthalmol.* **1992**, *230*, 505.